

## Response to RC2

Jan De Rydt, G. Hilmar Gudmundsson, Thomas Nagler, Jan Wuite, Edward C. King

4 December 2017

The authors present a collection of detailed observation data regarding the recent formation and propagation of two rifts in the BIS which may be crucial for its future. The first, called Chasm 1 by the authors, emerged and has been reactivated from a pattern of curved cracks and now propagates towards MIR. The second one is the Halloween crack which has been initiated near the MIR, and moves away from this spot rapidly. Based on numerical calculations in conjunction with the observed kinematical data, a prediction of the future rift propagation trajectories is made.

The observation data are of great value, as they provide, among others, a detailed insight into the kinematics of the crack propagation, the widening and the deformations near the rift tips. Also the numerical crack path predictions are interesting and I am sure that they will attract considerable attention. The paper is well written and clearly in most parts. In addition to these rather general remarks, I would like to make a few comments on points which have struck me.

We thank the review for these positive remarks and a constructive assessment of our work. Individual replies are formulated below, and all updated figures are listed at the end of this document.

- The main point is the following: I am not absolutely sure, but there seems to be an inconsistency between the velocity field as shown in Fig.7a and the obvious assumption that both cracks are pure mode I cracks. Figure 7a shows clear velocity jumps across the entire rifts in their normal as well as in their tangential direction which suggests a so-called mixed-mode loading. Such a mixed-mode loading would usually lead (homogeneity of the ice shelf presumed) to a crack curving (in this case to the left in propagation direction) and not to a nearly straight crack as predicted from the model. I wonder what the reasons for this apparent contradiction are. It might be that the velocity field is not sufficiently correct. But, on the other hand, this field has been used to optimize the model, i.e. the model results should show the same tendency. Perhaps the authors can resolve this question easily.

As the reviewer points out, it is difficult to discern a pure mode I from a mixed mode fracture based on the subsampled velocity data in Figure 7a. To provide evidence for a pure mode I, or at least a negligibly small mode II component, we have made the following changes to the manuscript:

- In Figure 2b we are showing strain rosettes around the tip of Chasm 1. These have been calculated using a network of 12 stakes, which have been monitored monthly using high precision GPS methods. The results provide strong evidence for extension across Chasm 1 rather than shear, i.e., a pure mode I loading.
- In Figure 4 a strain rosette was added based on the differential motion of GPS stations K0, L2 and H0 after the formation of the HC. Also here the principle

strain rate directions are oriented perpendicular and parallel to the rift, indicating limited shear.

- As the authors mention on page 15, the calculated principal stress trajectories have been used for crack path prediction instead of the measurable principal strain-rate trajectories because of the smoothening filter effect of the field equations. Here, a few explanations would be helpful, how this filter works and how its results depend on the input data as e.g. the measured velocity field. I wonder to what extent the filter may smoothen important observation facts like the velocity jumps.

We assume that the reviewer is referring to the regularization in the inversion, which determines the smoothness of the rate factor in Glen's flow law and prevents overfitting of the data. We have added the following statement to the manuscript:

“A Tikhonov regularization was used and the regularization multiplier,  $\lambda = 10^3$ , was determined through a L-curve approach to optimize the misfit and avoid overfitting. In areas away from the grounding line and the immediate vicinity of the MIR, the solution converged towards observed values of the surface velocities within 100 iterations, and the inversion was ended after 200 iterations.”

- On page 18 the authors mention that their propagation algorithm makes use of the direction of maximum tensile stress, but that the stress magnitudes are not a good indicator for the formation of new rifts or for predicting the future propagation. This statement might be correct, but this is not directly shown in this paper. In this context it should be emphasized that usual fracture criteria never use directly the stress magnitude and that the question of an appropriate fracture criterion is not touched in this paper.

We have added the following statement to the introduction:

“We do not intend to address the more complex issues of fracture initialization and the propagation speed of existing rifts, but rather present a heuristic algorithm for calculating rift trajectories once an initial fracture has formed.”

- Some more details regarding the used inversion method or the resolution of the measured velocity field and calculated stress field would have been helpful and interesting for the reader. For example, if available, one could use sufficiently accurate displacement-, velocity- or stress fields to check the applicability of different fracture criteria.

A detailed description of the inversion procedure is outside the scope of this work, but more information is available as part of the freely available model code for Úa ([ghg@bas.ac.uk](mailto:ghg@bas.ac.uk)). However, changes have been made to the text in order to address the sensitivity of the fracture trajectories to model details such as the mesh resolution:

“A priori, the calculated fracture trajectories depend on the amount of regularization ( $\lambda$ ) and the model resolution. Sensitivity tests were carried out for both variables and the final trajectories of the HC were found to be independent of the exact value of  $\lambda$  and mesh resolution. A further reduction of the regularization and additional mesh

refinement did not significantly change the results, and only for a much coarser mesh (2 km nodal separation) or a much larger amount of regularization ( $\lambda > 10^5$ ) did the modeled trajectories start to deviate from the observed trajectory. It should be noted that this result is case specific, and robustness of the fracture trajectories should be considered on a case-by-case basis, in particular for applications with a more complex stress distribution.”

- In Fig 2b caption and page 7: Though clear from the context, the term ‘local strain rate network’ may mislead some readers. Measured are not strains but relative displacements (widening per length). Furthermore, the white marked stakes are hardly distinguishable from the yellow O0/N0 markers. In R18: combing -> combining

Instead of ‘local strain network’ we now use ‘network of snow stakes’. However, differential motion of the stakes per distance and time is a strain rate per definition; hence such networks are commonly referred to as ‘strain rate network’ in the literature. We have changed the color of all markers to yellow and adjusted the caption accordingly.

- In Fig.7b and page 19: Again, though clear from the context, the term ‘effective strain’ may mislead some readers. In addition, it would have been more informative not to use x,y-coordinates, but local normal and tangential directions.

We do not understand why the term “effective strain rate” is misleading in this context. The standard definition of this scalar quantity, at least in glaciology, is given in line 8, page 13 (old version of the ms) and plotted in Figure 7b. If the reviewer is referring to the fact that fractures are present and therefore this is not a strain rate in the strictest ‘continuum mechanics’ sense, then we have added the following comment to the manuscript:

“Again it should be noted that these values also incorporate widening (Mode I) and shear (Mode II) of the rifts, and they are therefore not material strain rates in the strictest sense.”

- Fig.3b: I see the drawn black lines, but I cannot see the cracks (magnification problem?)

We have added two additional panels (d and e) to Figure 3 with a more detailed view of the fractures.

- P14, R24: ‘. . .based on the observed stresses. . .’: stresses have not been observed and cannot be observed directly! They may be calculated.

Terminology has been changed to “calculated”

- Multiple: ‘principle stress’ -> principal stress

done

- P15, R30-35: the details of the principal stress rosette pattern in the vicinity of MIR can only be seen if the figures are sufficiently magnified. It is indeed 'radial' but, strictly speaking, not symmetric since the radial principal stress changes its sign during circulating MIR. The pattern corresponds to that of a point force in a plate acting in the direction of the HC.

We have adjusted the spatial extent of Figures 8a and b in order to make the strain rosettes more visible. The text already mentions that "This pattern is generated by the point-interaction between the ice shelf and the bedrock at the MIR, and has resulted in the radially-outward growth of the HC, perpendicular to the tensile stresses.". We wonder if this is different from saying that the pattern corresponds to that of a point force in a plate, as suggested by the reviewer.

P3, R20-21: I agree fully with the opinion that observation data in conjunction with numerical simulations, as they are impressively presented by the authors, will improve the understanding of rift propagation and of the accuracy of relevant predictions. But I doubt the need for specific iceberg calving laws. The calving law is already known and given by the laws of continuum and fracture mechanics. The only and very difficult problem is to describe the rift evolution until final separation.

By 'calving law' we mean the formation and propagation of ice shelf rifts in the broadest sense, i.e. from rift initialization until iceberg formation. This process will be driven by the laws of fracture mechanics, which are well understood for a broad range of materials, but are little studied for ice shelves. Particular material properties and their spatial distribution (such as 'fracture toughness') are currently unknown for ice shelves, and it is unclear what determines whether/where rifts form and at what speed they propagate. Complex full-Stokes models with implemented fracture mechanics will be of help, but ultimately a more simplified set of 'calving criteria' will have to be developed for application in large-scale ice shelf models.

## UPDATED FIGURES

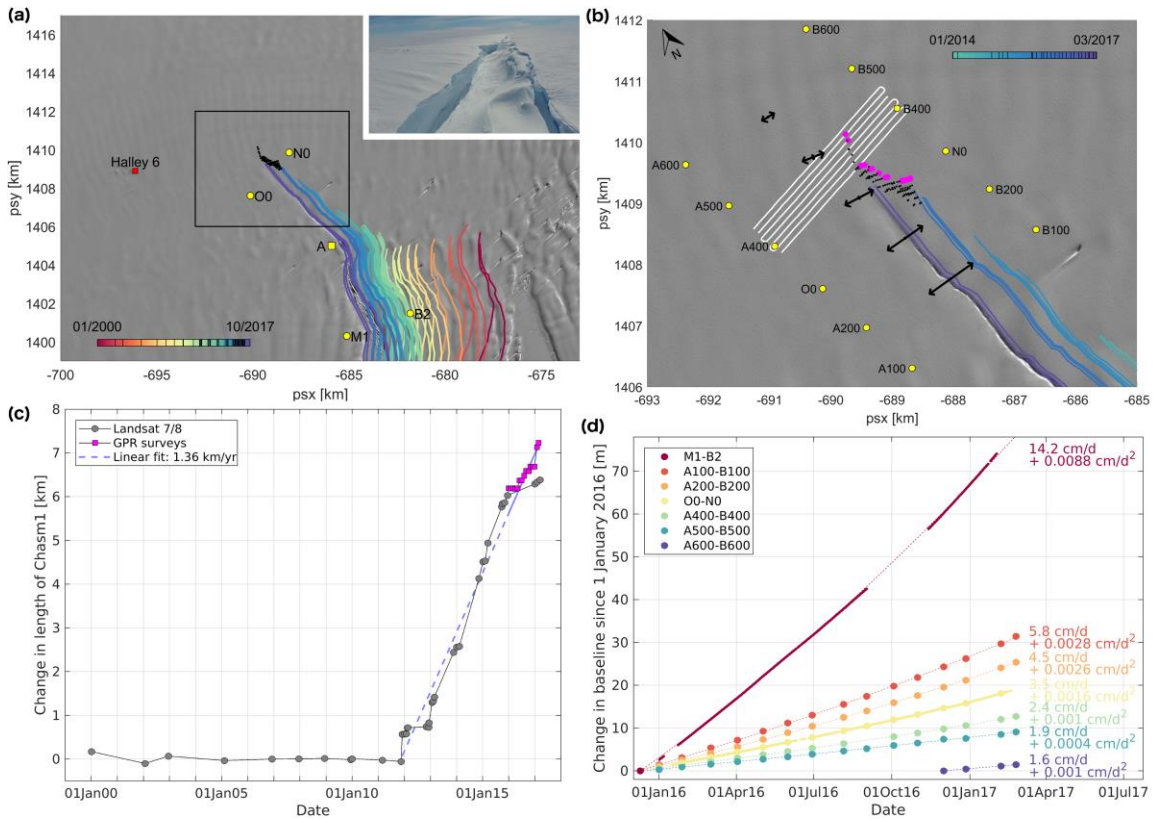


Figure 2. (a) Historical outlines of Chasm 1 from 6 January 2000 (red) to 15 March 2017 (purple), as the rift got advected by the ice flow. Outlines were obtained from a sequence of Landsat-7 and Landsat-8 panchromatic images, with acquisition dates as indicated by the black ticks in the colour bar. The background image is a subset of a Landsat-8 scene from 15 March 2017. The red dot indicates the location of Halley 6 research station, yellow dots are the locations of 4 permanent dual frequency GPS stations, and the black box outlines the extent of Figure b. The inset in the top right shows an aerial image of Chasm 1 taken in December 2015, looking from the reference point A towards the crack tip. (b) Detailed overview of the area around the tip of Chasm 1, showing the local snow stake network (yellow dots), an example of the GPR survey lines (white lines), and progression of the crack tip as obtained from satellite (blue-to-purple outlines) and GPR data (black dots). Strain rosettes were obtained from the relative movement of the snow stakes, and capture the widening of Chasm 1 as well as local strain rates in the ice shelf. (c) Propagation of the tip of Chasm 1 with respect to its historical location prior to the reactivation in December 2012, based on Landsat-7/8 images (grey markers), and monthly GPR surveys (magenta markers). A linear fit through all datapoints shows an average lengthening rate of the rift of 1.36 km/yr. (d) Baseline distance across Chasm 1 as a function of time, measured by two pairs of permanent GPS stations (O0-N0 and M1-B2 in (a)), and five pairs of snow stakes (A<sub>i</sub>-B<sub>i</sub>), with  $i \in \{100, 200, 400, 500, 600\}$  in (b)). The least-squares quadratic fit is plotted as a dashed line.

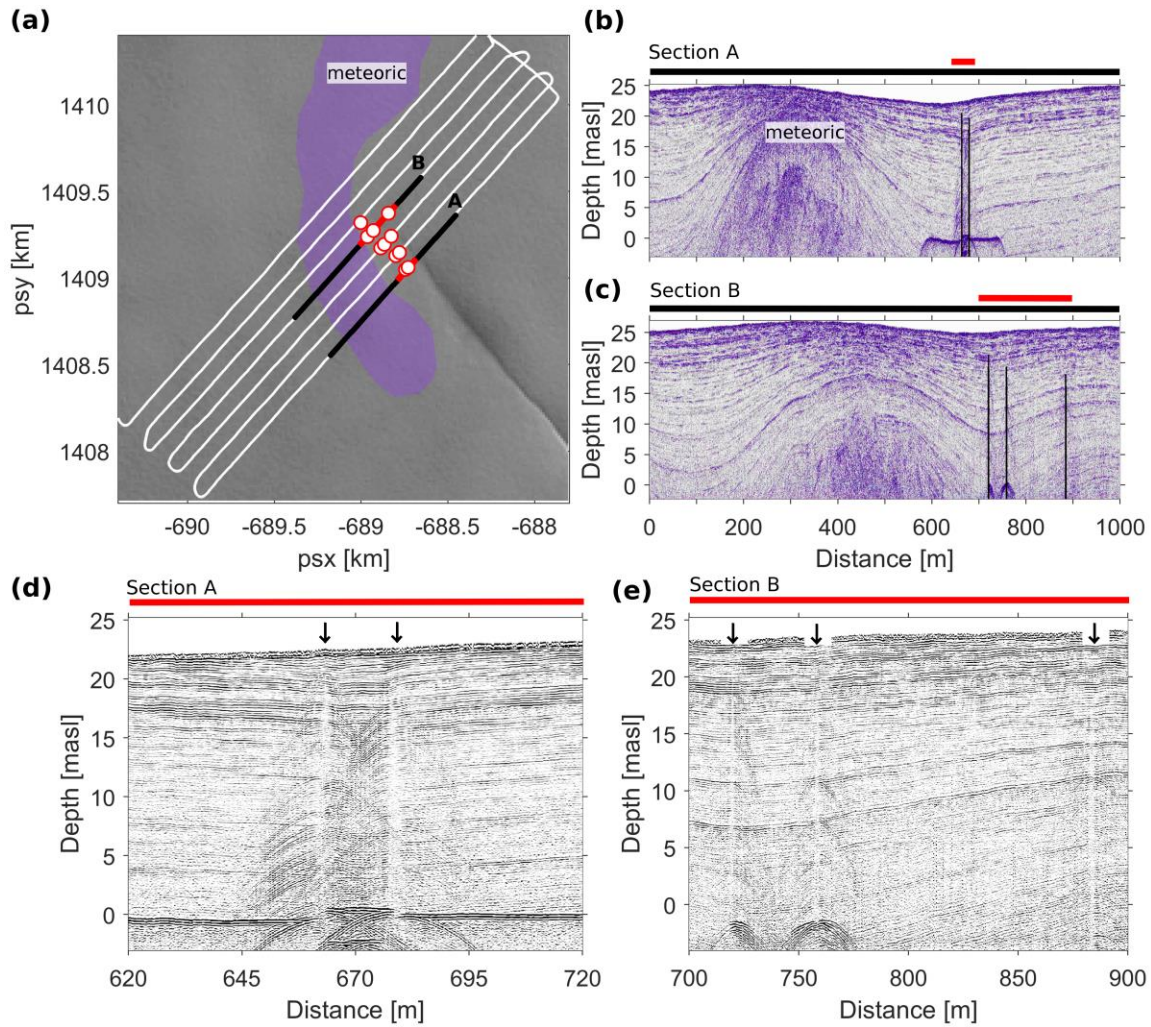


Figure 3. (a) GPS track of a GPR survey carried out on 4 May 2016 (white line), overlying a Landsat 8 image from 3 March 2016. Red dots correspond to locations where a fracture has been observed in the GPR data. Black line segments A and B correspond to the location of the radar sections displayed in Figures b and c respectively. The purple shading outlines the location of a large structure of meteoric ice embedded within the ice shelf (b) Radar section along line segment A in a. Vertical black lines indicate the location of fractures in the ice shelf. (c) Similar to b but for line segment B. (d) A detailed view of the fractures along section A. The spatial extent is indicated by the red line above panel b and vertical arrows locate the radar signature of each fracture. (e) Similar to d but for section B.

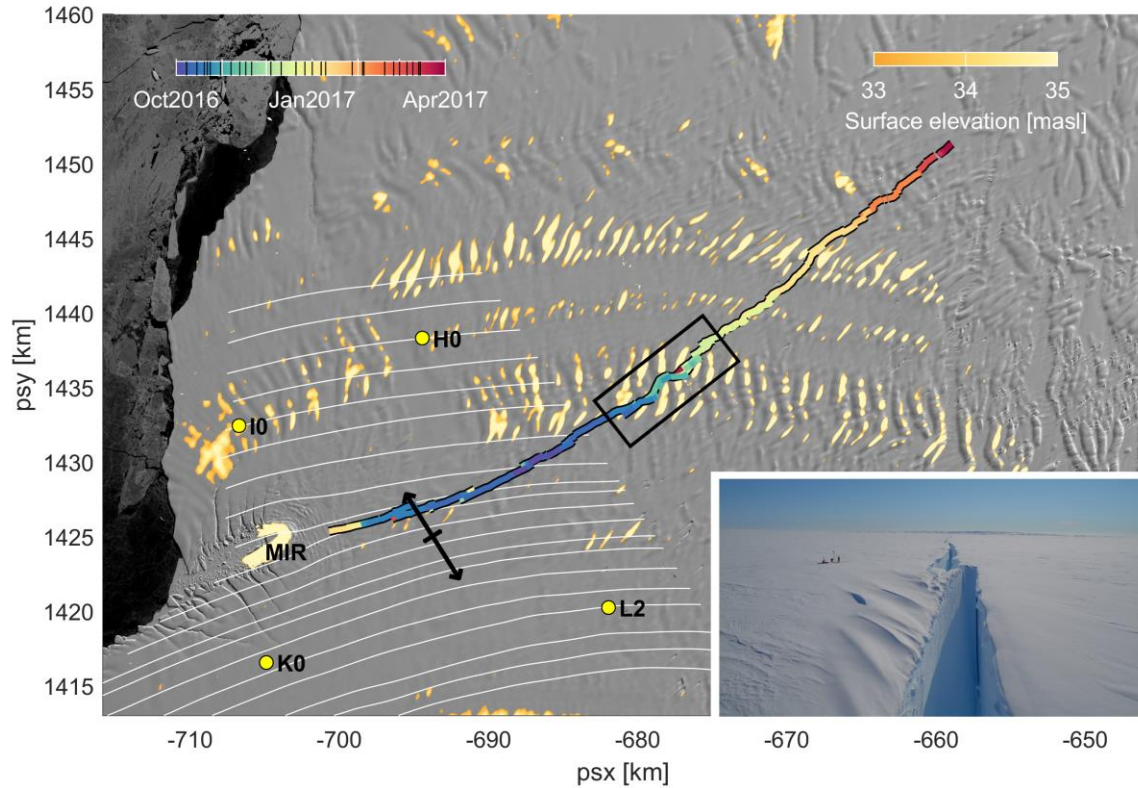


Figure 4. Extent of Halloween Crack (HC) based on a time series of manual outlines from Landsat-8 and Sentinel-2 images; the corresponding dates are indicated by black ticks in the colorbar. The background image is a Landsat-8 scene from 15 March 2017, yellow dots correspond to the location of 4 permanent GPS stations (K0, I0, H0 and L2), and the inset in the lower right shows an aerial image of the HC taken in January 2017 from a location 5 km to the east of the MIR. Orange-to-yellow colours highlight areas with a surface elevation above 33 m, and the black box outlines an area where the HC cuts through a band of thicker ice. White lines are flowlines based on a velocity field from 2015, prior to the formation of the HC, and indicate a localized divergence of flow around the MIR. The strain rosette is calculated from the differential motion of L2, K0 and H0 between 3 October 2016 and 1 February 2017.

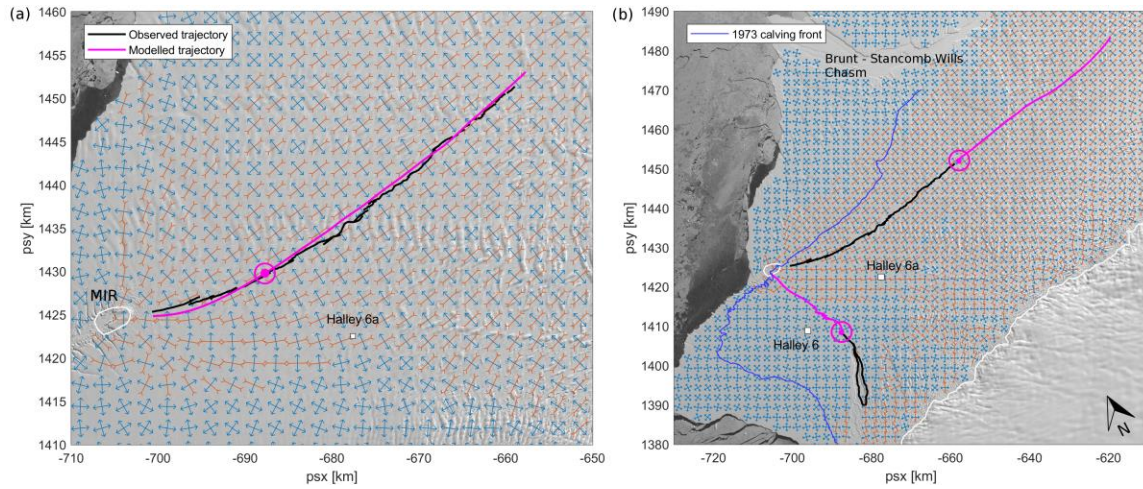


Figure 8. (a) Modelled principal stress components (red are compressive, blue are extensive) in June 2015, resampled on a regular 2.5 km by 2.5 km grid. The modelled trajectory of Halloween Crack based on the direction of maximal tensile stress is shown in magenta, the observed trajectory from 15 March 2017 is plotted in black. (b) Modelled principal stress components in March 2017 and predicted future trajectories of Chasm 1 and Halloween Crack. The purple line corresponds to the 1973 calving fro